analytical chemistry

Letter

pubs.acs.org/ac

Optomechanical Time-Gated Fluorescence Imaging Using Long-Lived Silicon Quantum Dot Nanoparticles

Wenzhao Yang,[†] Prateek K. Srivastava,[‡] Shanshan Han,[†] Lili Jing,[‡] Chang-Ching Tu,*,[†] and Sung-Liang Chen*,[†,§]

[†]University of Michigan-Shanghai Jiao Tong University Joint Institute, Shanghai Jiao Tong University, Shanghai 200240, China
[‡]School of Pharmacy, Shanghai Jiao Tong University, Shanghai 200240, China
[§]State Key Laboratory of Advanced Optical Communication Systems and Networks, Shanghai Jiao Tong University, Shanghai 200240, China

S *Supporting Information*

ABSTRACT: We demonstrate a novel optomechanical synchronization method to achieve ultrahigh-contrast time-gated fluorescence imaging using live zebrafish as models. Silicon quantum dot nanoparticles (SiQDNPs) with photoluminescence lifetime of about 16 μs were used as the long-lived probes to enable background autofluorescence removal and multiplexing through time-gating. A continuous-wave 405 nm laser as the excitation source was focused on a rotating optical chopper on which the emission light beam obtained from an inverted fluorescence microscope was also focused but with a phase difference such that in a short delay after the excitation laser is blocked, the emission light beam passes through the optical chopper, initiating the image acquisition by a conventional sensor. Both excitation and detection time windows were synchronized by one optical chopper, eliminating the need for pulsed light source and image intensifier which is often used as ultrafast optical shutter. Through use of the cost-effective time-gating method, nearly all background autofluorescence emitted from the yolk sac of a zebrafish embryo microinjected with the SiQDNPs was removed, leading to a 45-fold increase in signal-to-background ratio. Furthermore, two kinds of fluorescence signals emitted from the microinjected SiQDNPs and the intrinsic green fluorescent protein of transgenic zebrafish larvae can be clearly separated through time-gating.
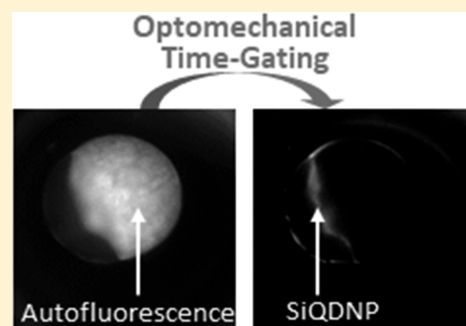
Fluorescence imaging is an indispensable tool in biomedical research. It helps visualize fluorescence signals emitted from various endogenous or exogenous fluorophores in biological samples at macro- to nanoscale.[1−4] When exogenous probes such as organic dyes and semiconductor quantum dots are used for immunofluorescence imaging, endogenous autofluorescence as background noise interferes with the actual fluorescent signals, decreasing the contrast and thus the accuracy of diagnosis. One straightforward method to avoid such background interference is to move the desired luminescence spectrum into the near-infrared (NIR) window, typically ranging from 650 to 900 nm, where the autofluorescence is minimal.[5] However, NIR-fluorescing organic dyes such as indocyanine green (ICG) are often susceptible to photobleaching,[6] causing stability issues particularly for long-term or time-lapse investigations. Another method to suppress background autofluorescence is so-called time-gated imaging, in which following each excitation pulse, the signal acquisition does not start immediately, but rather shortly delays until the short-lived autofluorescence (lifetime <10 ns) fully diminishes. As a result, only the long-lived luminescence originating from the exogenous probes is collected for imaging.

In this work, we use highly fluorescent silicon quantum dot nanoparticles (SiQDNPs) as long-lived probes for time-gated

fluorescence imaging. Compared to other long-lived probes composed of either rare earth or transition metals such as europium, ruthenium, and lanthanide complexes,[7−9] silicon-based nanomaterials are generally more biocompatible.[10,11] The SiQDNPs were synthesized by a novel top-down method developed previously (Figure S1).[10] The SiQDNPs have majority overall particle sizes ranging from 100 to 200 nm (Figure S2A) and are characterized by their irregular shapes and mesoporous surfaces (Figure S2B), to which clusters of crystalline silicon quantum dots of sizes about 5 nm are attached (Figure S2C). Here, all the SiQDNPs are functionalized with sulfonate (Figure S3), which provides excellent water solubility for consistent microinjection to the zebrafish embryos or larvae. The SiQDNP suspension in water shows broad excitation range from 300 to 500 nm and strong absorption in the ultraviolet range (Figure S2D). Under 365 nm excitation, the SiQDNP suspension emits intense red photoluminescence (PL) with a peak wavelength located at 626 nm (Figure S2D), and the PL quantum yield was measured to be 5.3% (Figure S4).

Furthermore, the PL of the SiQDNP suspension has a long lifetime of about 16 μs (Figures S2E and S5) as a result of radiative recombination of photoexcited charge carriers through the oxide-related surface defects associated with the Si−O−Si bonds,[12,13] which normally show strong infrared absorption from 950 to 1300 cm^{-1} (Figure S3). The *in vitro* cell viability assay reveals that the sulfonate-terminated SiQDNPs have inhibitory particle concentration corresponding to 50% cell viability (IC$_{50}$) more than 640 μg/mL (Figure S6), which is much higher than the IC$_{50}$ of other cadmium-based quantum dots (about 10 to 20 μg/mL),[11] confirming the biocompatibility of the SiQDNPs.

In general, a conventional fluorescence imaging system can be converted to a time-gated one by integration with a pulsed light source and an image intensifier for photon multiplication and as an ultrafast shutter. As a representative example, a standard epifluorescence microscope, after being incorporated with an intensified charge-coupled device (ICCD) and a xenon flash lamp, was able to perform time-gated cellular imaging with nearly all background luminescence removed.[9] Although showing high performance, such system requires the use of highly expensive ICCD, which generally costs significantly more than a common CCD and needs complex electronic synchronization control.[14,15] In other implementations, although no necessity of ICCD, a pulsed excitation source along with sophisticated timing control is still essential.[16−19] It is worth mentioning that the fluorescence lifetime imaging method (FLIM) can also remove background autofluorescence effectively and at the same time allows for time-domain multiplexing.[20,21] However, to obtain the time-resolved fluorescence decay of each pixel, a standard FLIM setup must be equipped with manifold functionalities such as X−Y scanning, time-correlated single photon counting (TCSPC), and single photon detection. Therefore, the system is inevitably complicated and costly, and the image acquisition process is relatively time-consuming.

In this work, we present a simple, cost-effective, and high performance time-gated fluorescence imaging system based on a novel optomechanical synchronization method for which only a nonintensified imaging sensor and a continuous-wave (CW) laser for excitation are used, as illustrated in Figure 1. The excitation light beam produced from a 405 nm CW laser diode first passes through a focusing lens and then a pinhole to yield a focus (spot size about 0.8 mm) on a rotating optical chopper. During the excitation time window, the excitation light beam further travels through the optical chopper and enters into an inverted fluorescence microscope after reflection by a beam splitter. The excitation light power measured at the back entry port of the microscope is about 50 mW. The fluorescence microscope is equipped with a bandpass excitation filter (395−415 nm), a long-pass dichroic mirror (>460 nm), and a long-pass emission filter (>475 nm) which, in combination, are suited for the 405 nm excitation and allow the entire fluorescence spectrum of the SiQDNPs to be collected for imaging. During the detection time window, the emission light beam emitted from the side exit port of the microscope is first focused on the optical chopper (spot size about 1 mm) by one focusing lens, then collimated by the other, and lastly enters into a nonintensified complementary metal−oxide−semiconductor (CMOS) imaging sensor after passing through another beam splitter. The above excitation−detection cycle continues to repeat as long as the chopper keeps on rotating. Meanwhile, the CMOS imaging sensor integrates the fluorescence signals
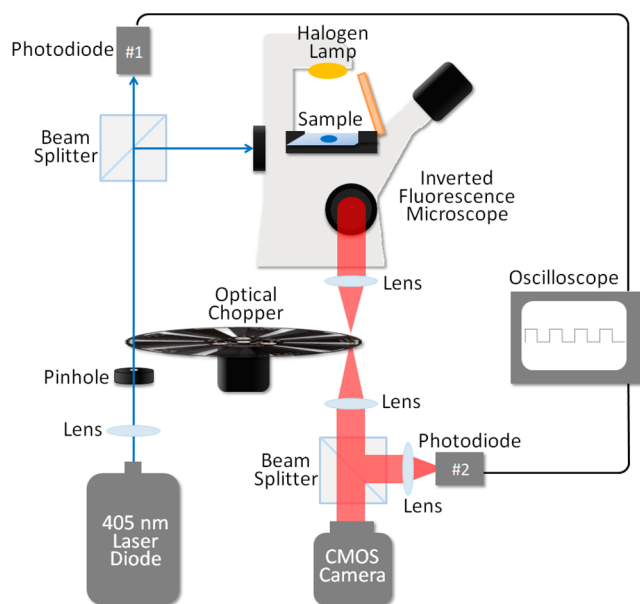

Figure 1. Schematic of the optomechanical time-gated fluorescence imaging system.

obtained in each cycle over a certain time period until a good signal-to-background ratio is achieved. The working principle of the optomechanical time-gating method using single optical chopper is further explained in detail in Figure S7. With a finite focus size, the process of a light beam being blocked by or passing through the chopper occurs in a gradual manner rather than instantaneously. Given that the two foci were of size about 1 mm and the optical chopper (10-slot blade, duty cycle 40% and diameter 101.6 mm) rotated at a speed of 5100 rpm, the resulting excitation and detection time windows were measured using the two photodiodes in Figure 1, and a 20 μs delay, which is sufficient for all short-lived luminescence to fully decay, was determined experimentally (Figure S8). Because the SiQDNP fluorescence intensity drops about 75% after the 20 μs delay, a relatively long (about 500 to 3500 ms) exposure time of the CMOS imager was used for the time-gated fluorescence image acquisition.

To demonstrate the time-gating capability of the optome-chanical time-gated fluorescence imaging system, fluorescein isothiocyanate (FITC) and SiQDNPs were put side by side for imaging (Figure 2). A droplet of concentrated sulfonate-terminated SiQDNP suspension in water was placed in adjacent to a mixture of FITC and epoxy resin. Because the resin is hydrophobic and resistant to water, a clear boundary line which separates the FITC area from the SiQDNP area is formed. Under the non-time-gated mode (Figure 2A and 2B), the FITC area shows an average fluorescence intensity 5 times higher than that of the SiQDNP area, which can be converted to a signal-to-background ratio = 0.2, assuming that the SiQDNP fluorescence is considered as the signal and the FITC fluorescence as the background. As a comparison, taking an image at the same location but under the time-gated mode (Figure 2C and 2D), the signal-to-background ratio increases to 6.86, which is equivalent to about 34-fold improvement. Particularly, if only the green marked area on the FITC side and the red marked area on the SiQDNP side are considered, the signal-to-background ratio increases from 0.34 in the non-time-gated mode to 117.68 in the time-gated mode, leading to about 346-fold improvement. In addition, the fine surface features on the SiQDNP side which
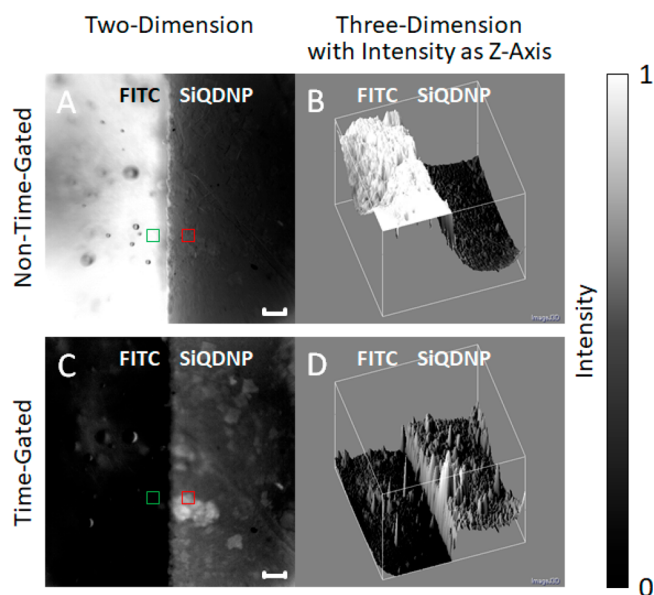
Figure 2. (A and B) Nontime-gated and (C and D) time-gated fluorescence images in two- and three-dimension with intensity as *z*-axis of FITC and SiQDNP, respectively. Objective lens of 10-times magnification was used. Two-dimensional images have resolution of 1100 ×1100 pixels. Green and red marked areas have size of 40 × 40 pixels. Scale bar is equal to 100 μm. The CMOS imager exposure time was 5 and 600 ms under the non-time-gated and time-gated modes, respectively. The optical chopper rotational speed was kept at 5100 rpm under the time-gated mode.

are initially overshadowed by the exceedingly large FITC fluorescence under the non-time-gated mode become clearly visible after switching to the time-gated mode.

Zebrafish embryos have been widely used as animal models to study vertebrate embryology, mainly because of their optical transparency, which enables direct investigation of internal development of the living embryos from outside. However, the embryos, particularly at the yolk sac parts, usually carry strong autofluorescence, which is hard to remove by using optical filters due to its wide spectral distribution (Figure S9).[22] Here, we demonstrate nearly complete removal of autofluorescence by using the optomechanical time-gated fluorescence imaging system and the sulfonate-terminated SiQDNPs as long-lived fluorescent probes. Prior to imaging, about 5 nL of the SiQDNP suspension in water (1 mg/mL) was microinjected to the embryonic cells of a living AB strain wild-type zebrafish embryo, as indicated by the red arrow in Figure 3A. Noteworthily, no obvious adverse effect to the embryo was observed after the microinjection. Under the non-time-gated mode (Figure 3B and 3C), the microinjected SiQDNPs are essentially not visible due to the dominant autofluorescence emitted from the nearby yolk sac, and the signal-to-background ratio, here estimated as the average fluorescence intensity within the red marked area versus the green marked area in Figure 3B, is as low as 0.58. As a comparison, under the time-gated mode (Figure 3D and 3E), the distribution of the microinjected SiQDNPs among the embryonic cells can be clearly observed because the background autofluorescence was effectively removed by time-gating. As a result, the signal-to-background ratio drastically increases to 26.07, yielding about 45-fold improvement. Equipped with such an outstanding background removal character, the optomechanical time-gated fluorescence imaging system developed in this work can be a promising platform for biological research on

zebrafish such as lineage tracing and fluorescence imaging[23,24] and for clinical applications such as sentinel lymph node mapping.[11] Although *in vivo* time-gated fluorescence imaging on mice with more than 100-fold signal-to-background ratio improvement using similar luminescent porous silicon nanoparticles has been demonstrated,[25] the time-gating of the reported imaging system was realized by employing much more expensive ICCD and pulsed excitation sources.

In addition to the background removal, we also demonstrated time-domain multiplexing, i.e. separating long-lived fluorescence signals from short-lived ones, by using the optomechanical time-gated fluorescence imaging system. Different from the AB strain wild-type zebrafish embryo shown in the previous example, here we used GFP transgenic zebrafish larvae as the demonstration model in which the intrinsic green fluorescence makes the internal structures such as vascular system easily observable from outside. Through microinjection (5 nL of 1 mg/mL) at the head, yolk sac, and tail parts of the larvae, as indicated by the red arrows in Figure 3F, 3K, and 3P, respectively, we put the SiQDNPs in adjacent to the GFP which has PL lifetime in nanoseconds. The microinjection did not result in any significant adverse effect to the living larvae. By comparing the non-time-gated fluorescence images (Figure 3G, 3L, and 3Q) alongside with the time-gated ones (Figure 3I, 3N, and 3S), the long-lived signals coming from the SiQDNPs can be clearly distinguished from the short-lived ones of GFP. Interestingly, except the tail demonstration (Figure 3S), the majority of the SiQDNP signals were found displaced from the original microinjection sites at the head and yolk sac (Figure 3I and 3N), which can be attributed to the diffusion and transportation of the SiQDNPs through the lymphatic systems. As the controlled experiment, larvae without microinjection of the SiQDNPs did not show any fluorescence signals in the time-gated mode (Figure S10). While autofluorescence might also be included in the non-time-gated images here, its intensity was found weaker than the GFP fluorescence experimentally and is mainly located at the yolk sac part (Figure S10). Nevertheless, either GFP or autofluorescence can be effectively removed under the time-gated mode, and such complete separation of signals can only be achieved in the time-domain by time-gating because, in the wavelength-domain, their PL spectra are at least partly overlapped with each other (Figure S9). Besides the zebrafish models, cellular imaging using the system was also demonstrated on SKOV3 and CHO cells, in which short-lived fluorescence signals from the Hoechst dye stained at the cell nuclei were entirely removed, again manifesting the time-gating ability of the system (Figure S11).

In summary, we demonstrate a novel optomechanical time-gated fluorescence imaging system which can achieve ultrahigh contrast at low cost. Based on a conventional epifluorescence microscope, the time-gating functionality is mainly accomplished by one optical chopper with no need of expensive ICCD, pulsed light source, or complex synchronization control. In the system, both the excitation light beam from a 405 nm CW laser and the emission light beam from the fluorescence microscope are focused on one rotating optical chopper, and the two foci are positioned with a phase difference such that in a 20 μs delay after the excitation laser is blocked, the emission light beam passes through the optical chopper, initiating image acquisition by a CMOS imager. Here, we used biocompatible and highly water-soluble SiQDNPs, which have long fluorescence lifetime in about 16 μs, as the long-lived probes and zebrafish as demonstration models. Under the time-gated mode, nearly all
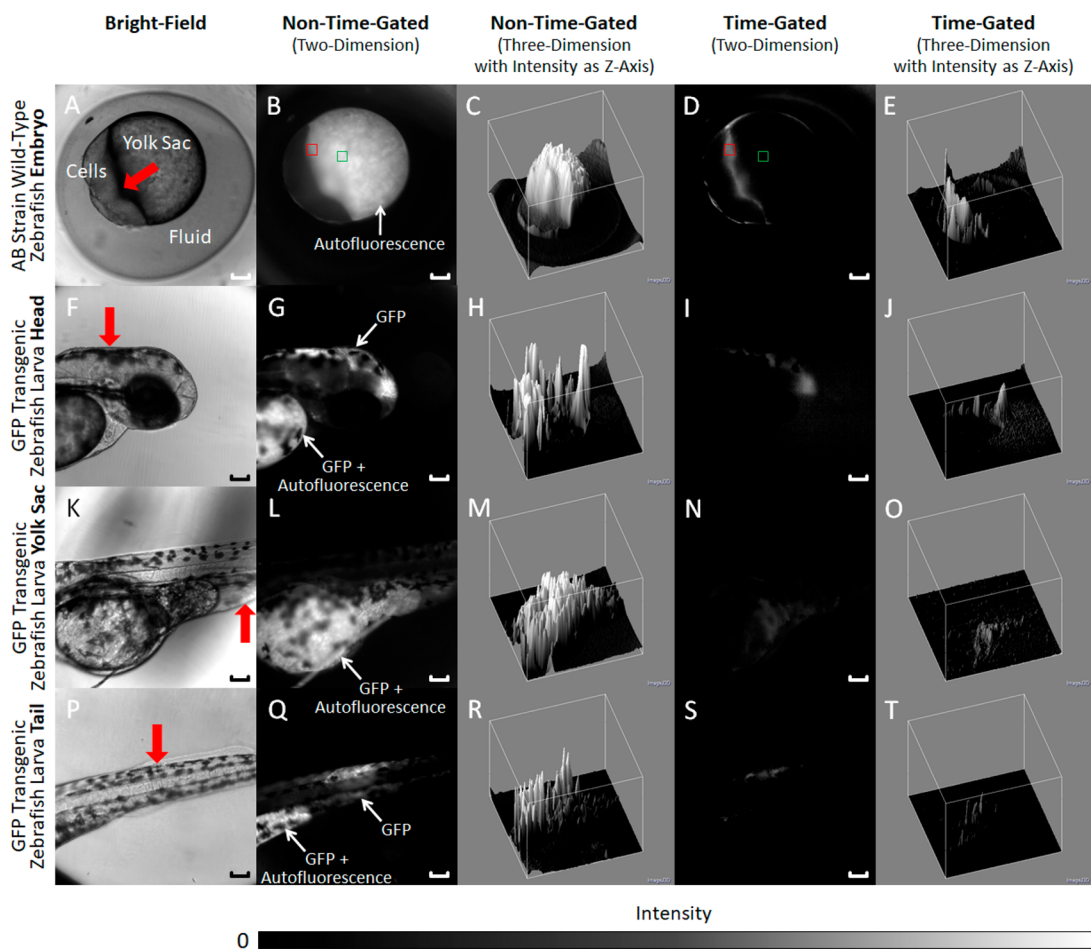
Figure 3. (A, F, K, P) Bright-field images of zebrafish embryo and larvae microinjected with SiQDNPs. The microinjection sites and directions are indicated by the red arrows. (B, G, L, Q) Nontime-gated fluorescence images in two-dimension and (C, H, M, R) their corresponding three-dimensional images with intensity as *z*-axis of the microinjected zebrafish embryo and larvae. (D, I, N, S) Time-gated fluorescence images in two-dimension and (E, J, O, T) their corresponding three-dimensional images with intensity as *z*-axis of the microinjected zebrafish embryo and larvae. Objective lens of 10× magnification was used for all images. The scale bars are equivalent to 100 μm. In panels B and D, the two-dimensional images have resolution of 1280 × 1280 pixels, and the red and green marked areas have size of 40 × 40 pixels. The CMOS imager exposure time was about 400 and 3500 ms under the non-time-gated and time-gated mode, respectively. The optical chopper rotational speed was kept at 5100 rpm under the time-gated mode.

background autofluorescence emitted from the yolk sac of a zebrafish embryo microinjected with the SiQDNPs was removed, leading to a 45-fold increase in signal-to-background ratio. Furthermore, by comparing the non-time-gated fluorescence images alongside with the time-gated ones, the intrinsic GFP fluorescence signals of transgenic zebrafish larvae can be clearly separated from the exogenous fluorescence signals emitted from the microinjected SiQDNPs. Owing to its cost-effectiveness and compatibility with standard fluorescence imaging methods, the optomechanical time-gated fluorescence imaging system developed in this work can be potentially applied to a wide range of biological research and diagnostics applications.

■ ASSOCIATED CONTENT

Ⓢ Supporting Information

The Supporting Information is available free of charge on the ACS Publications website at DOI: 10.1021/acs.anal-chem.9b00517.

Synthesis and characterizations of the SiQDNPs; PL quantum yield and the PL lifetime of the SiQDNPs; FTIR spectra of the SiQDNPs with different surface chemistry; cell viability assay for the SiQDNPs; working principle of the optomechanical time-gating method; experimentally measured excitation and detection time windows; PL spectra of GFP, autofluorescence, and the SiQDNPs; bright-field, non-time-gated, and time-gated fluorescence images of zebrafish larvae without microinjection of the SiQDNPs and SKOV3 and CHO cells stained with the Hoechst dye (PDF)

■ AUTHOR INFORMATION

Corresponding Authors

*E-mail: sungliang.chen@sjtu.edu.cn; Tel.: +86-21-34206765 Ext. 4281.
*E-mail: changching.tu@sjtu.edu.cn; Tel.: +86-21-34206765 Ext. 5081.

ORCID Ⓘ

Chang-Ching Tu: 0000-0002-9233-1928

Author Contributions

C.-C.T. and S.H. proposed the original idea and performed synthesis and characterization of SiQDNPs and preparation of

the final manuscript. S.-L.C. and W.Y. implemented and optimized the optical system and performed image acquisition and composition of the first manuscript draft. L.J. and P.K.S. prepared the biological samples.

Notes

The authors declare no competing financial interest.

■ REFERENCES

(1) Lichtman, J. W.; Conchello, J.-A. *Nat. Methods* **2005**, *2*, 910−919.

(2) Helmchen, F.; Denk, W. *Nat. Methods* **2005**, *2*, 932−940.

(3) Sahl, S. J.; Hell, S. W.; Jakobs, S. *Nat. Rev. Mol. Cell Biol.* **2017**, *18*, 685−701.

(4) You, S.; Tu, H.; Chaney, E. J.; Sun, Y.; Zhao, Y.; Bower, A. J.; Liu, Y.-Z.; Marjanovic, M.; Sinha, S.; Pu, Y.; Boppart, S. A. *Nat. Commun.* **2018**, *9*, 2125.

(5) Weissleder, R. *Nat. Biotechnol.* **2001**, *19*, 316−317.

(6) Resch-Genger, U.; Grabolle, M.; Cavaliere-Jaricot, S.; Nitschke, R.; Nann, T. *Nat. Methods* **2008**, *5*, 763−775.

(7) Li, M.; Selvin, P. R. *J. Am. Chem. Soc.* **1995**, *117*, 8132−8138.

(8) Song, C. H.; Ye, Z. Q.; Wang, G. L.; Jin, D. Y.; Yuan, J. L.; Guan, Y. F.; Piper, J. *Talanta* **2009**, *79*, 103−108.

(9) Hanaoka, K.; Kikuchi, K.; Kobayashi, S.; Nagano, T. *J. Am. Chem. Soc.* **2007**, *129*, 13502−13509.

(10) Tu, C.-C.; Chen, K.-P.; Yang, T.-A.; Chou, M.-Y.; Lin, L. Y.; Li, Y.-K. *ACS Appl. Mater. Interfaces* **2016**, *8*, 13714−13723.

(11) Erogbogbo, F.; Yong, K.-T.; Roy, I.; Hu, R.; Law, W.-C.; Zhao, W.; Ding, H.; Wu, F.; Kumar, R.; Swihart, M. T.; Prasad, P. N. *ACS Nano* **2011**, *5*, 413−423.

(12) Dohnalová, K.; Poddubny, A. N.; Prokofiev, A. A.; de Boer, W. D.; Umesh, C. P.; Paulusse, J. MJ; Zuilhof, H.; Gregorkiewicz, T. *Light: Sci. Appl.* **2013**, *2*, No. e46.

(13) Kůsová, K.; Cibulka, O.; Dohnalová, K.; Pelant, I.; Valenta, J.; Fučíková, A.; Žídek, K.; Lang, J.; Englich, J.; Matějka, P.; Štěpánek, P.; Bakardjieva, S. *ACS Nano* **2010**, *4*, 4495−4504.

(14) Bouccara, S.; Fragola, A.; Giovanelli, E.; Sitbon, G.; Lequeux, N.; Pons, T.; Loriette, V. *J. Biomed. Opt.* **2014**, *19*, 051208.

(15) Connally, R.; Piper, J. *J. Biomed. Opt.* **2008**, *13*, 034022.

(16) Jin, D.; Piper, J. A. *Anal. Chem.* **2011**, *83*, 2294−2300.

(17) Zhang, L.; Zheng, X.; Deng, W.; Lu, Y.; Lechevallier, S.; Ye, Z.; Goldys, E. M.; Dawes, J. M.; Piper, J. A.; Yuan, J.; Verelst, M.; Jin, D. *Sci. Rep.* **2015**, *4*, 6597.

(18) Zheng, X.; Zhu, X.; Lu, Y.; Zhao, J.; Feng, W.; Jia, G.; Wang, F.; Li, F.; Jin, D. *Anal. Chem.* **2016**, *88*, 3449−3454.

(19) del Rosal, B.; Ortgies, D. H.; Fernández, N.; Sanz-Rodríguez, F.; Jaque, D.; Rodríguez, E. M. *Adv. Mater.* **2016**, *28*, 10188−10193.

(20) Mandal, G.; Darragh, M.; Wang, Y. A.; Heyes, C. D. *Chem. Commun.* **2013**, *49*, 624−626.

(21) Tu, C.-C.; Awasthi, K.; Chen, K.-P.; Lin, C.-H.; Hamada, M.; Ohta, N.; Li, Y.-K. *ACS Photonics* **2017**, *4*, 1306−1315.

(22) Shi, X.; Teo, L. S.; Pan, X.; Chong, S.-W.; Kraut, R.; Korzh, V.; Wohland, T. *Dev. Dyn.* **2009**, *238*, 3156−3167.

(23) Hsu, Y.-C. *Stem Cells* **2015**, *33*, 3197−3204.

(24) Kang, Y.-F.; Li, Y.-H.; Fang, Y.-W.; Xu, Y.; Wei, X.-M.; Yin, X.-B. *Sci. Rep.* **2015**, *5*, 11835.

(25) Joo, J.; Liu, X.; Kotamraju, V. R.; Ruoslahti, E.; Nam, Y.; Sailor, M. J. *ACS Nano* **2015**, *9*, 6233−6241.